CrossMark

ORIGINAL ARTICLE

Three-dimensional shock wave diffraction off a discontinuous edge

S. Cooppan[1] · B. Skews[1]

Abstract The interaction of three-dimensional vortex flows was investigated through vortex shedding off a discontinuous edge. Two wedges of 14.5° wedge angle (up and downstream edges) were separated by an offset. The size of the offset (5, 10, and 20 mm) and the Mach number (Mach 1.32, 1.42, and 1.6) were the key parameters investigated. Experimental images were taken and computational simulations were run; a close relation was found between the two. This enabled the three-dimensional effects of the flow to be studied and analysed. It was found, as the offset increased in size, the vortices shed off the up and downstream edges took a longer time to merge and the strength of the interaction was weaker. The vortex topology changed with a larger offset; the downstream vortex was thinner (in terms of cross-sectional diameter) adjacent to the offset, which is an indication of a change in density, than the rest of the vortex along the downstream diffraction edge. This particular feature was more prevalent at lower Mach numbers. The effect of a higher Mach number was to increase the rate of dissipation of the vortices, lengthen the shear layer due to the higher upstream velocity, and make the vortex profile elliptical.

Keywords Shock diffraction · Vortex shedding · Unsteady flow

✉ B. Skews
beric.skews@wits.ac.za

1 Flow Research Unit School of Mechanical Industrial and Aeronautical Engineering, University of the Witwatersrand, PO WITS, Johannesburg 2050, South Africa

1 Introduction

Over the last half-century there has been extensive research into two-dimensional vortices shed by a diffracting shock wave around a corner. The developments of technology in computational fluid dynamics (CFD) and high speed cameras has allowed for the study of vortex dynamics in three dimensions. The work done by Sun and Takayama [1] has shown that detailed and accurate models can be created to simulate shock wave diffraction in two dimensions and this can now be extended. The common practice is a pictorial comparison of the numerical solutions with experimental images.

The primary features of two-dimensional shock wave diffraction have been well established following the early work in [2]. These are: the free vortex, shear layer, viscous vortex, reflected expansion wave, and the diffracted shock wave. The presence of a secondary shock wave was identified at high shock Mach numbers and is addressed in detail in [3]. This occurs when the incident shock Mach number is greater than 1.35 and results from the reflected expansion wave accelerating the flow above the curved shear layer to supersonic velocities.

In more recent times, there have been studies of three-dimensional flows. Reeves [4] investigated unsteady three-dimensional compressible vortices generated by passing shocks (of various strengths) over diffraction edges of different profiles. The shapes included a V, an inverted V, as well as parabolic and inverted parabolic models. The vortices expand in time and bend significantly near the test section window to meet it at 90°, since it is a solid boundary. For the V models, the vortex assumed a conical shape as the shock wave propagated over the edges with signs of disruption where they met at the apex of the V. This paper analysed a number of factors, such as tangential and radial velocity and normalised pressure. Particular attention was paid to where kinks and bends

develop in the vortex profile resulting in reduced diameter and increased vorticity. There was evidence to suggest that the vorticity production was independent of the diffracting edge profile, since the plot of normalised pressure against time only varied with Mach number. The shear layer lengthens and the vortex takes on an elliptical profile in time, with this being more marked with an increase in Mach number. Two other conclusions were reached: one, that the circulation is proportional to time and, two, that the rate of circulation is proportional to the shock strength.

An exploratory study [5] of shock-induced vortex shedding over a discontinuous edge formed the precursor to the current work with the setup and typical result given in Fig. 1. The photograph clearly shows the difference in position of the diffracted wave from the two edges, but the termination of the wave and the vortex shed from the upstream edge is obscured by the downstream surface. The surface of the merging of the shocks and vortices is not evident. This issue is overcome in the current study. Simulations of this ear-
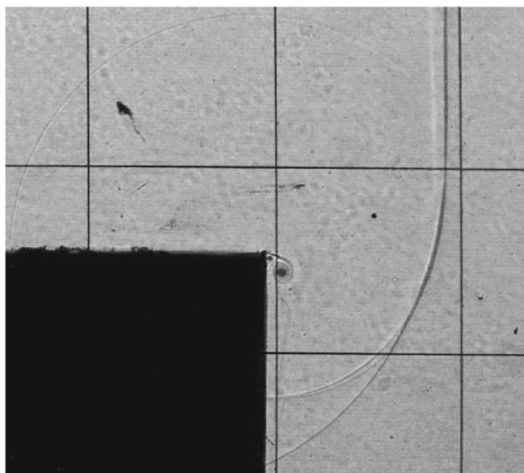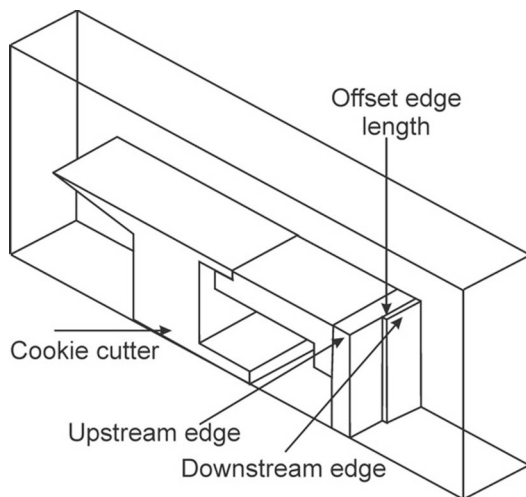
lier geometry indicated areas requiring further study of these aspects.

A more recent preliminary study [6] has examined the flow field resulting from the interaction between the diffraction flows arising from the interaction of two shock waves generated from two independent shock tubes having a common diffraction edge. Only the synchronous case was looked at with emphasis on the intersection of the two shed vortices. The above studies have highlighted the need for a closer examination of the diffraction flows over surfaces and edges such as would be found in shock propagation over structures, such as buildings.

2 Method

2.1 Experimentation

Tests were conducted in a conventional shock tube at Mach numbers of 1.32, 1.42, and 1.6. The tube is operated in double-diaphragm mode, with a small intermediate chamber, resulting in the production of reproducible Mach numbers with a variation of ± 1 % of the preset value. The test section is 180 mm high and 76 mm wide. The test pieces were attached to the same cookie cutter as used previously [4] with new diffraction inserts with wedge angles of 14.5° as indicated in Fig. 2. It is known that such large flow turning angles (165.5°) have no effect on the separated flow pattern and in this case allow visualisation of the vortices shed from both edges. Offset edge lengths of 5, 10, and 20 mm were used. This range of values was chosen to firstly show the strong interaction between the vortices shed off the upstream and downstream edges and thereafter to see the diminishing interaction, up until the vortices behaved independently.
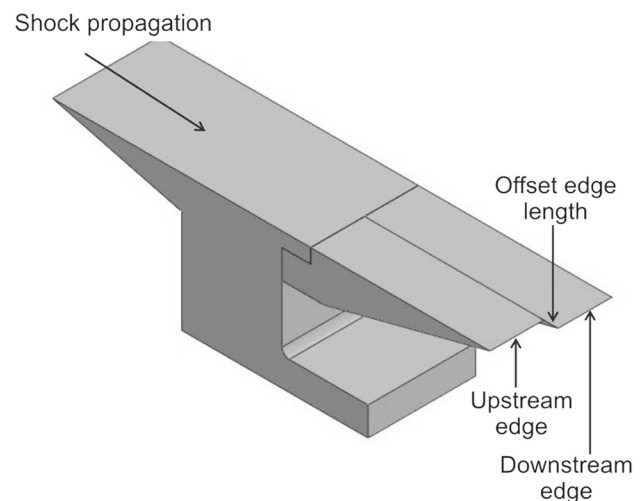

Fig. 1 Initial experimental arrangement and shadowgraph for a 10 mm edge offset

Fig. 2 Experimental test piece

Flow visualisation was a typical Z-arrangement optical system for both schlieren and shadowgraph imaging, using a 12 megapixel camera and a flash exposure time of 2 μs.

2.2 Numerical simulation

The flow domain was made the same physical size as the physical test volume. Since the volume around the diffraction edges was the key area of interest, they were fitted with a separate cylindrical volume of much higher resolution. Fluent$^{©}$ was used as the CFD package with two levels of adaption. Initial cell sizes of 5, 3.5, and 2.5 mm were used to test for grid independence. The total cell count varied from 908,623 to 1,406,394 for these cases. Because of strong similarities, the coarser mesh was used. Contours of density and Y-velocity were plotted on the x–y-plane, i.e., the plane perpendicular to the optical axis, corresponding to that of the shadowgraph image in Fig. 1. The shapes of the diffracted shock were clearly defined in the density contours for all three models. As with the density contours, the Y-velocity contours show little to no variation across the different mesh sizes. Both quadrilateral and unstructured meshes were tested and it was found that the unstructured mesh gave better resolution in the region of the vortices. The standard $k - \epsilon$ turbulence model was implemented and gave very similar results to an inviscid solution. The adequacy of the numerical simulation was judged based on comparisons with the experimental results and previous work.

A comparison between experiment and simulation is given in Fig. 3. The CFD image is made up of slices taken through the x–y-plane, the density contours in colour are at the nearest face of the fluid domain (looking into the page), whereas the density contours in black are furthest away. Iso-surfaces of density are plotted to show the vortex geometry. The experimental shadowgraph shows close correspondence with the two shock profiles that are those closest to the windows on either side of the shock tube where they are still plane and uninfluenced by the model offset. The shed spiral vortices are evident and show profiles in the region where they are still two dimensional and unaffected by the offset.

3 Results

3.1 Shed vortices

The main focus of this section is the topology of the free vortices, namely what effect does Mach number and offset edge length have on vortex shape and structure. The results are presented in accordance with the Mach number, starting at Mach 1.32 and ending at Mach 1.6. The Mach 1.32 images are taken with a schlieren setup and the others with shadowgraph. The experimental images are displayed with the different test
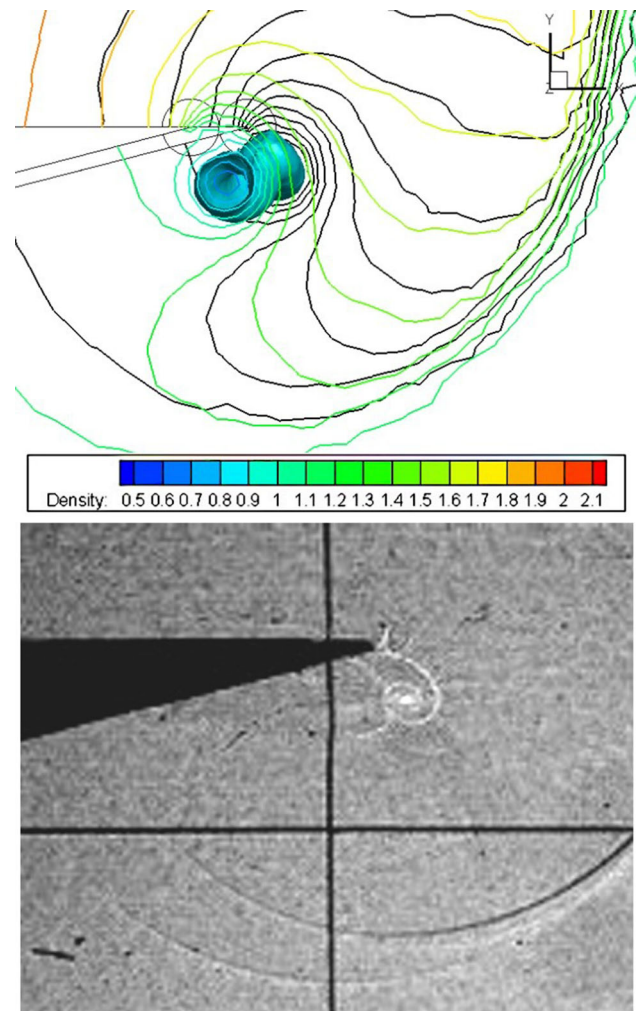

Fig. 3 Numerical simulation and shadowgraph image of the diffraction pattern of a Mach 1.42 incident shock off the 5 mm offset edge length test piece at a time of 75 μs

pieces next to each other, with the 5 mm model on the left, 10 mm model in the centre and 20 mm model on the right. The time quoted in the images refers to the time taken after the shock has diffracted over the upstream edge. Whilst a large number of results and images are available, only some will be presented here.

3.1.1 Results for M = 1.32

A selection of schlieren images is given in Fig. 4 for the three test pieces and various times. At early times, a vortex is shed from the upstream edge before the shock wave has encountered the downstream edge.

As with previous similar studies [4], the vortices end on a surface, similarly to vortices in inviscid incompressible flows. Thus, the portion of the vortex passing adjacent to the offset edge attaches to the underside of the adjacent test piece, or at very early times to the vertical face of the offset

Fig. 4 Experimental schlieren images of shock diffraction for a Mach 1.32 incident shock wave at times of 30, 66, and 100 μs
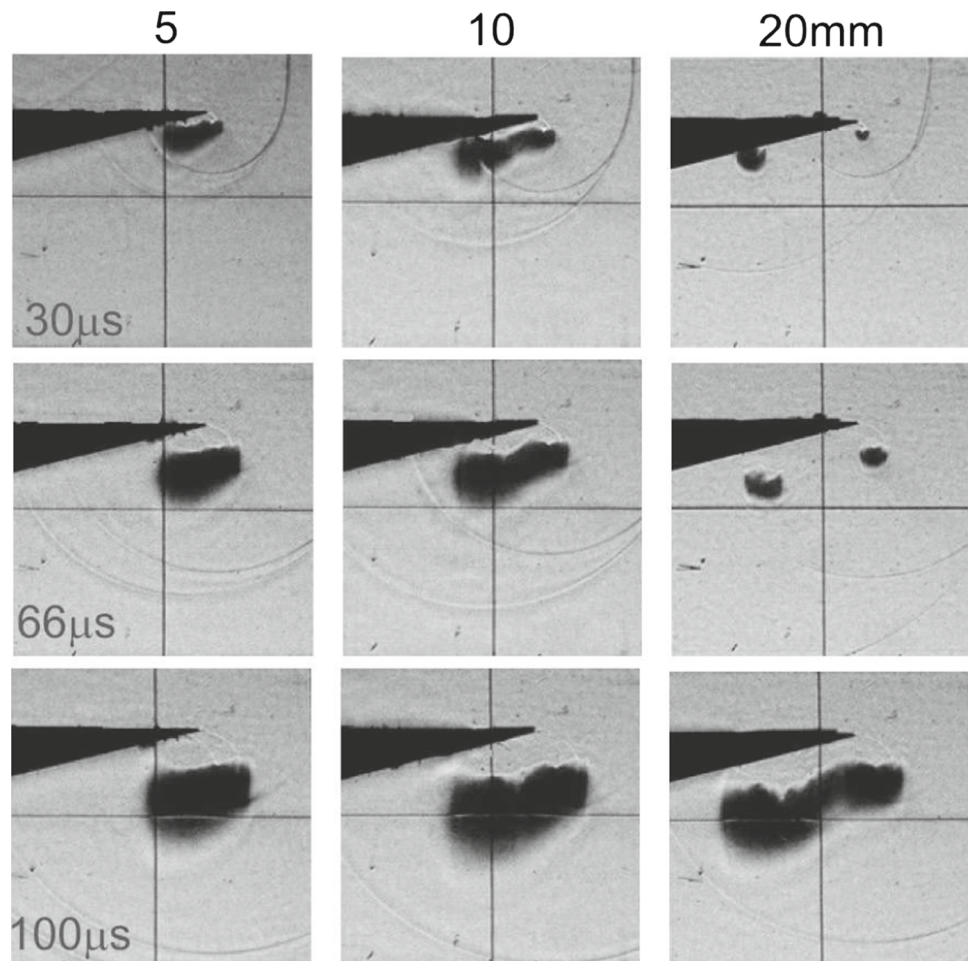
edge, whilst the other end terminates on the window. There is an indication of this in the top row of Fig. 4. At the same time, there will be some flow over the offset edge due to the high pressure behind the advancing shock and the lower pressure on the other side of the offset edge resulting from the expansion following the upstream edge diffraction. Once the shock passes over the downstream edges, the second vortex is shed which will interact with this flow. The main portion will be the normal two-dimensional diffraction pattern positioned ahead of the vortex from the upstream edge, behaving independently of it. As time progresses, the interaction will become more complex with the vortices amalgamating and will propagate in transverse directions from the offset edge position. For the different offset edge lengths, amalgamation occurs at different times, although it is difficult to judge from the images when and how this will be as it is affected by the sensitivity of the schlieren system. The trajectories of the two-dimensional part of the vortices is downward and to the right with that of the upstream edge being further advanced having been shed earlier.

Greater clarity is obtained from the numerical simulations. The variations of isosurfaces of density with regard to shape and structure are presented in Fig. 5. Two density surfaces are plotted; one at 0.8 kg/m^3 and the other at 1.1 kg/m^3. There are rapid changes in shape of the isosurfaces, and in some cases the surface terminates along the vortex axis. This occurs where the density drops below the set value as it decreases toward the vortex core. Thus, in the case of the 10 and 20 mm offset lengths at 30 μs, the density drops below the lower set value and a gap appears in the representation. The figure shows the impact the offset edge length has on the vortices shed off the upstream and downstream edges. There is a significant effect at the downstream edge. The size of the portion of the vortex adjacent to the discontinuity is significantly reduced. There is an inverse relationship between the size of this part of the vortex and the size of the offset edge length, the larger the discontinuity the smaller (in terms of proportional cross-sectional diameter) is the corresponding unaffected portion of the vortex. There is a more significant change in density for a larger offset edge length. It is also noted in the upper images how the upstream shed vortex curls around to terminate on the underside of the downstream wedge. Features such as stretching, twisting, and curvature of the merged vortex around the discontinuity can be seen in both the com-

Fig. 5 Isosurfaces of density of 0.8 kg/m³ on the inner surface and 1.1 kg/m³ on the outer surface, at time delays (*top* to *bottom* rows) of 10, 30, 56, and 108 μs, for a Mach number of 1.32
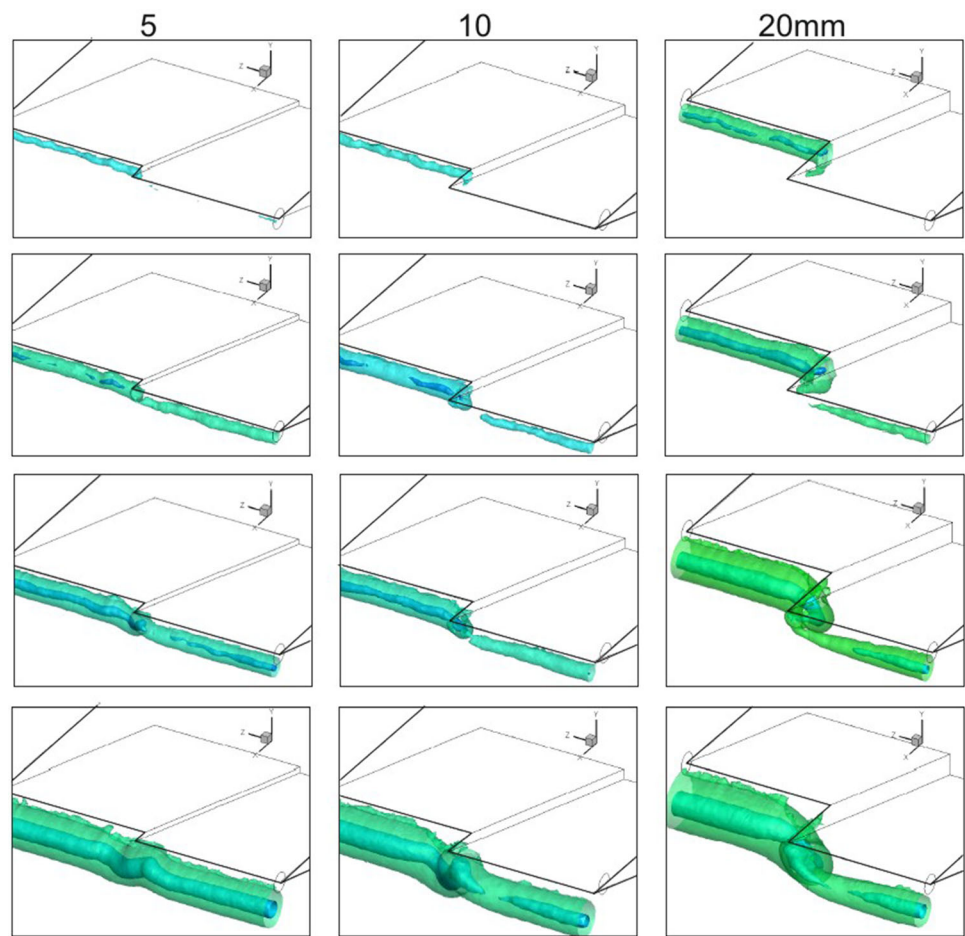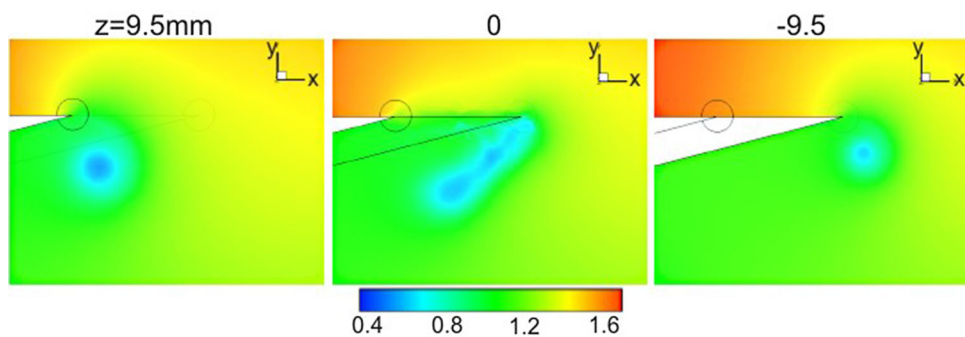

Fig. 6 *x–y* plane density plots. The *centre* image is at the offset edge and the other two at 9.5 mm either side with the upstream edge case on the *left*, for a Mach number of 1.32


putational and experimental set of images. From both the experimental and numerical images, it appears that as the vortices merge they take on a somewhat "S"-shaped profile, winding up together in a complex manner. For the larger density isosurface, there is also evidence of the shear layer arising from the wedge apex, which wraps up into the vortex.

Density contour slices taken in the *x–y* plane at distances of 9.5 mm on either side of the plane passing through the offset edge, as well as at the edge itself are shown in Fig. 6 at a time of 109 μs. The larger vortex from the upstream edge (left image) is evident, as it has been in existence longer than that

shed from the downstream edge (right image). The density field in the plane of the offset edge is complex, showing a few areas of low density as the vortex core winds through the plane. Low density persists all the way to the wedge tip before moving down to the two-dimensional vortex in the right image. This movement is not evident in the schlieren images due to the sensitivity of the system and the weaker gradients.

It is clear that the flow around and at the offset edge is complex. Figure 5 shows that there is a major change in the density distribution as well as in the shape of the density

Fig. 7 Vorticity in the *x–y* plane situated at the offset edge for three offset edge lengths and times of 10, 27, and 65 µs, and a Mach number of 1.32
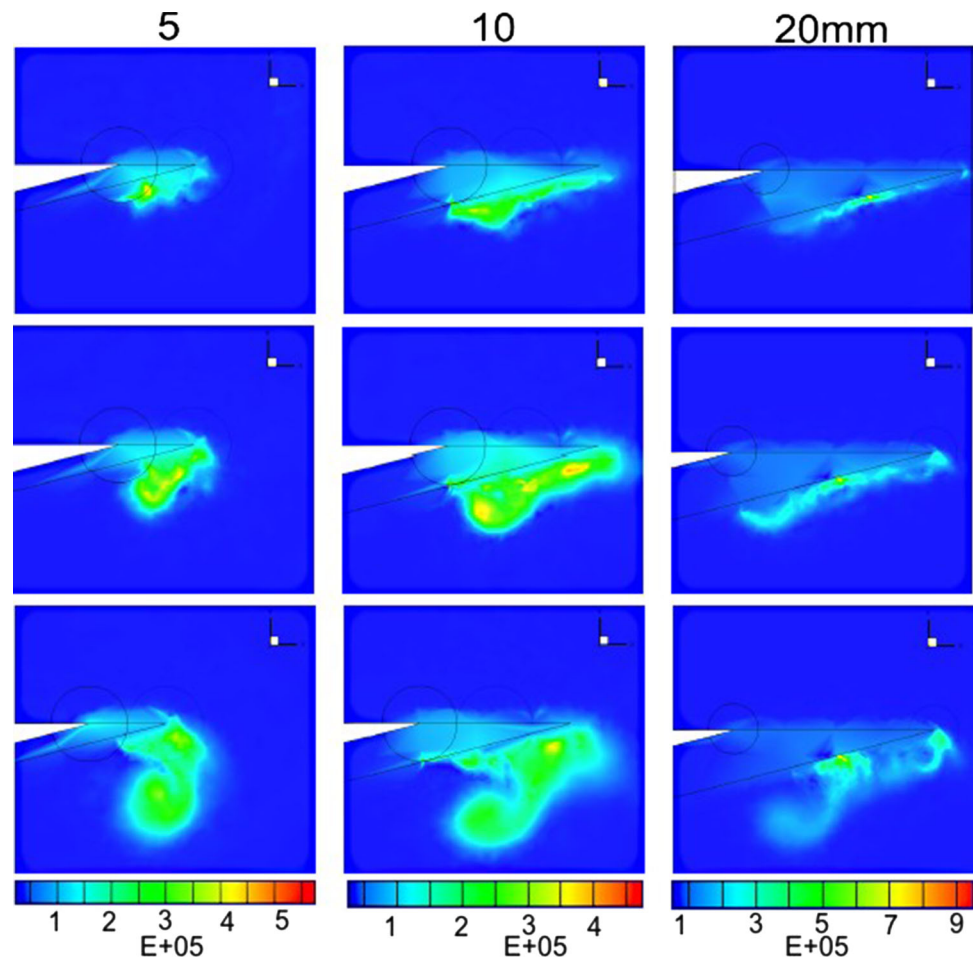

contours about the discontinuous edge; see Fig. 6 (centre image).

Figure 7 gives the vorticity plots in the *x–y* plane passing through the offset edge for the three offset lengths at increasing times. These show that besides the vortices shed off the two transverse edges, they are also shed off the offset edge. This occurs even before the shock has passed over the downstream edge and results from the sideways flow component induced on the upper surface due to the transverse pressure gradient as described earlier. As this vortex moves away, the vorticity remaining is due to the shear layer which continues to shed off the edge. With regard to the connectedness of the topology, it could be assumed that for large offset lengths, the upstream and downstream vortices would behave independently for some time, both wrapping around to terminate on the underside of the model. However, the situation is complicated by the transverse flow off the offset edge itself which will interact with the other two, since there are three edges in the geometry. Figures 6 and 7 give indications of this connectedness. Thus, the issue of connectivity in the topology will require a more detailed study. Also, a more comprehensive study of the flows on the upper sur-

faces resulting from the expansion waves generated due to shock diffraction would be needed to quantify these effects. The vorticity magnitude reaches a peak at some point in time and afterward begins to drop. For the limited data presented, this occurs for the 10 mm offset edge length at 27 µs. The vorticity magnitude is lower at the same time for a larger offset edge length.

Further insights about the behaviour of the flow about the offset edge lengths are obtained from analysing slices along the *y–z* and *x–z* planes. Figure 8 shows the *Y*-direction velocity in the *y–z* plane at a time of ≈53 µs for the three offset edge lengths. The starting position is at the downstream edge and the ending position at the upstream edge. The positions are numbered numerically, i.e., 1 at the downstream edge and 5 at the upstream edge. The slices taken cover the length of the offset. The distance between each slice is evenly spaced: 5 mm for the 20 mm model, 2.5 mm for the 10 mm model, and 1.25 mm for the 5 mm model. Colours should not be compared between the three different offset edge lengths, since the velocity range changes; however, they can be compared for each length. As the length increases in size, the velocity of the vortex shed of the upstream edge drops. As the

Fig. 8 *Y*-velocity contours in the *y*–*z* plane taken along the offset edge length at a time of 53 μs, and a Mach number of 1.32
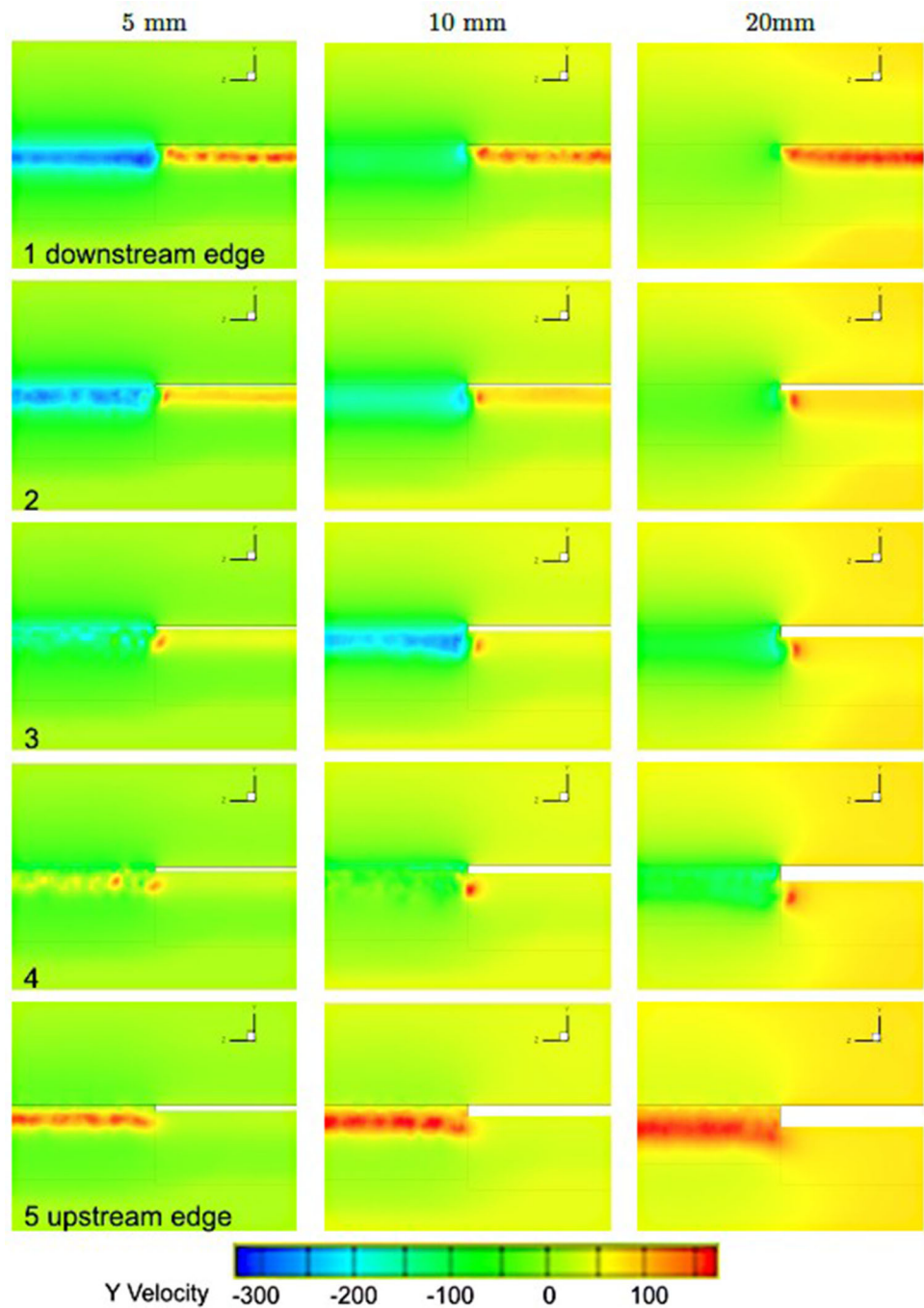

imaging plane passes through the vortex core, the direction of velocity will reverse. This feature is demonstrated by the 5 mm model in positions 1 and 5, and positions 3 and 5 for the 10 mm model.

An interesting feature is when the edge length increases in size, a larger portion of the upstream vortex is attached to the underside of the model. At a time of 53 μs, the downstream vortex has formed and is situated away from the downstream edge due to the shear layer. The downstream vortex is the largest in terms of magnitude for the 20 mm model

(position 1). The implication is that as the offset edge length increases in size, firstly the vortices behave more independently and, secondly, the offset edge length has less effect on the structure of the up and downstream vortices, away from the edge.

Contours of *Z*-velocity are analysed and presented in the same manner as the *Y*-velocity contours. Position 1 in Fig. 9 is where the upstream and downstream edges are flush on the upper surface of the wedges. Position 5 is lower with the distance between the slices for the 20, 10,

Fig. 9 Z-velocity contours in the *x–z* plane taken along the offset edge length at a time of 53 μs, and a Mach number of 1.32
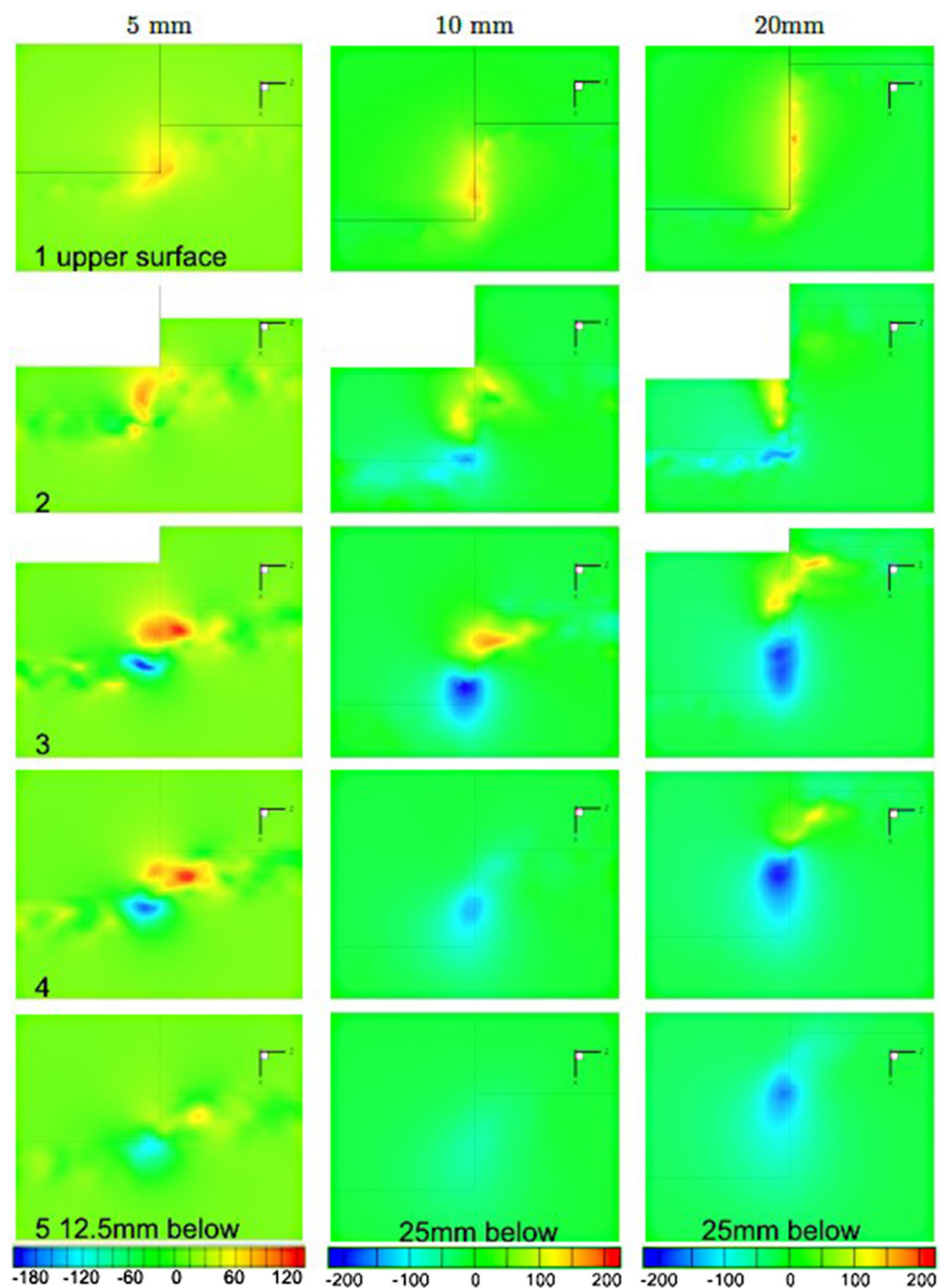

and 5 mm models being 25, 25, and 12.5 mm, respectively.

Position 1 demonstrates what has already been established and that which can intuitively be implied; the larger the edge length, the longer is the size and shape of the contours, as can be seen from positions 1–5. The 5 mm model has most contours with an orange/red colour, whereas the 20 mm model has most contours which are blue. Given the scale and colour scheme, this shows that the colour change of the contours from a small to a large offset is an indication of the change in direction along the *Z* axis of the *Z*-velocity for different sized offset edge lengths.

For all three models, the highest velocity occurs at either position 3 or 4. These positions are in close proximity to the underside of the model. Figure 5 shows that the isosurfaces of density off the upstream edge curve downwards at the edge length before joining with the isosurfaces from the downstream edge. A combination of the above two characteristics show that a major change to the flow occurs near the underside of the model. In addition, the isosurfaces of den-

Fig. 10 Experimental shadowgraph images of shock diffraction for a Mach 1.42 incident shock wave at times of 23, 45, 67, and 86 μs
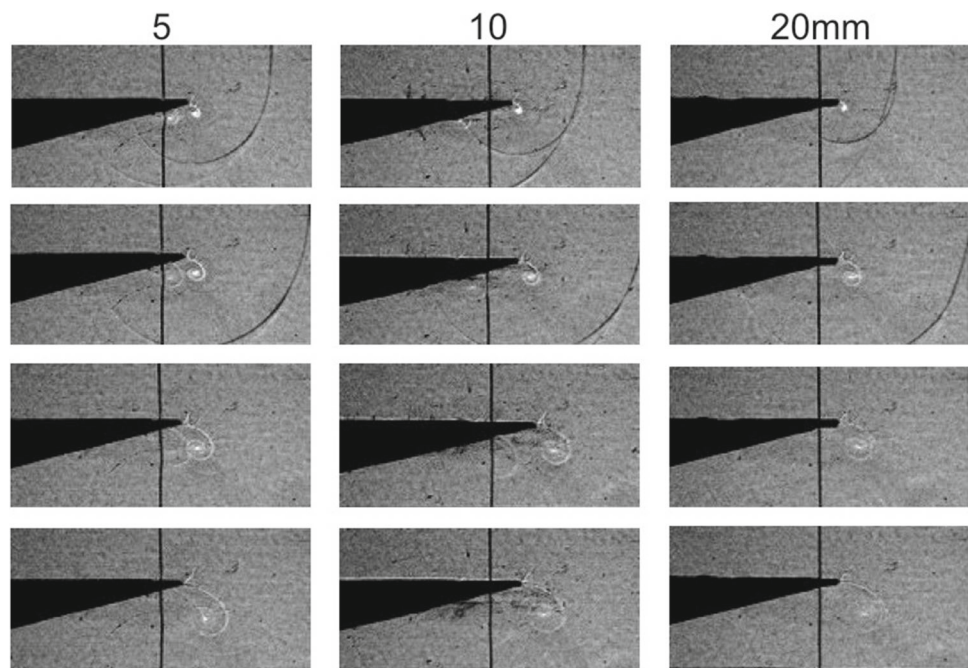
sity also show a more complex shape about the edge length as the offset edge length increases in size. This is complemented by the increasing size of the Z-velocity contours for larger offsets, as it is an indication of changes in direction and magnitude of velocity at a given position.

3.1.2 Results for $M = 1.42$

The experiments at this Mach number were done with shadowgraph imaging, giving different insight into the vortex shape and structure, as shown in Fig. 10. The vortex shed of the downstream edge can be seen clearly for all three models. The upstream vortex is less visible in the images with a higher offset edge length. This is partly due to the fact that for a larger length, the flow has expanded more. Furthermore, a part is obscured by the shadow of the downstream edge.

In general, the main features of the flow are similar to those at Mach 1.32. The main difference is the appearance of shocklets at Mach 1.42. The shocklets are not seen for the upstream vortex as the shocklets appear on the shear layer, which is hidden by the model for all three offset edge lengths. The primary cause for the formation of shocklets is the development of transonic flow above the shear layer. This is a well-known feature in two-dimensional studies.

The density isosurfaces are shown in Fig. 11. At early times, they are not as smooth, presumably due to the development of the shocklets. Reeves [4] found that an increase in Mach number caused a lengthening of the shear layer and an elliptical profile for the free vortices, noted here as well. As expected, the flow develops more rapidly in the case of Mach 1.42. The 20 mm model has larger changes in den-

sity for Mach 1.32 in comparison to Mach 1.42. As seen in Fig. 12, the vorticity shed at the offset edge is similar to that for the Mach 1.32 case except that the similarity occurs at earlier times, because of the higher gas velocity as evident in comparing the patterns at 63 μs in the Mach 1.32 case with that at 34 μs for Mach 1.42.

The 5 mm model shows what seems to be a merged vortex with a large shear layer, which is an indication of the strong interaction of the vortices from the up and downstream edges. On the other hand, there is a clearer distinction between the flow from the up and downstream edges than for the 20 mm model.

3.1.3 Results for $M = 1.6$

Because of the higher post-shock velocity compared to the previous cases, the shear layer and vortex grow much faster. A distinguishing feature compared to the previous cases is the appearance of lambda shock configurations, evident in Fig. 13. These are more developed forms of the shocklets found at the lower Mach number. In Reeves' three-dimensional study [4], these were found at Mach 1.65, but secondary and tertiary shocks were also found. For the two-dimensional case, secondary shocks are present at Mach 1.35 [1]. In the current study, there is some evidence of these in the vicinity of the shear layer and vortex, particularly at early times and for the shorter offsets.

There are more irregularities on the iso-surfaces for Mach 1.6 than for previous Mach numbers, as shown in Fig. 14. These are as a consequence of the shocklets and the development of instabilities in the shear layer. They also

Fig. 11 Isosurfaces of density of 0.8 kg/m^3 on the inner surface and 1.1 kg/m^3 on the outer surface, at time delays (*top* to *bottom* rows) of 8, 34, 62, and 106 µs, and a Mach number of 1.42
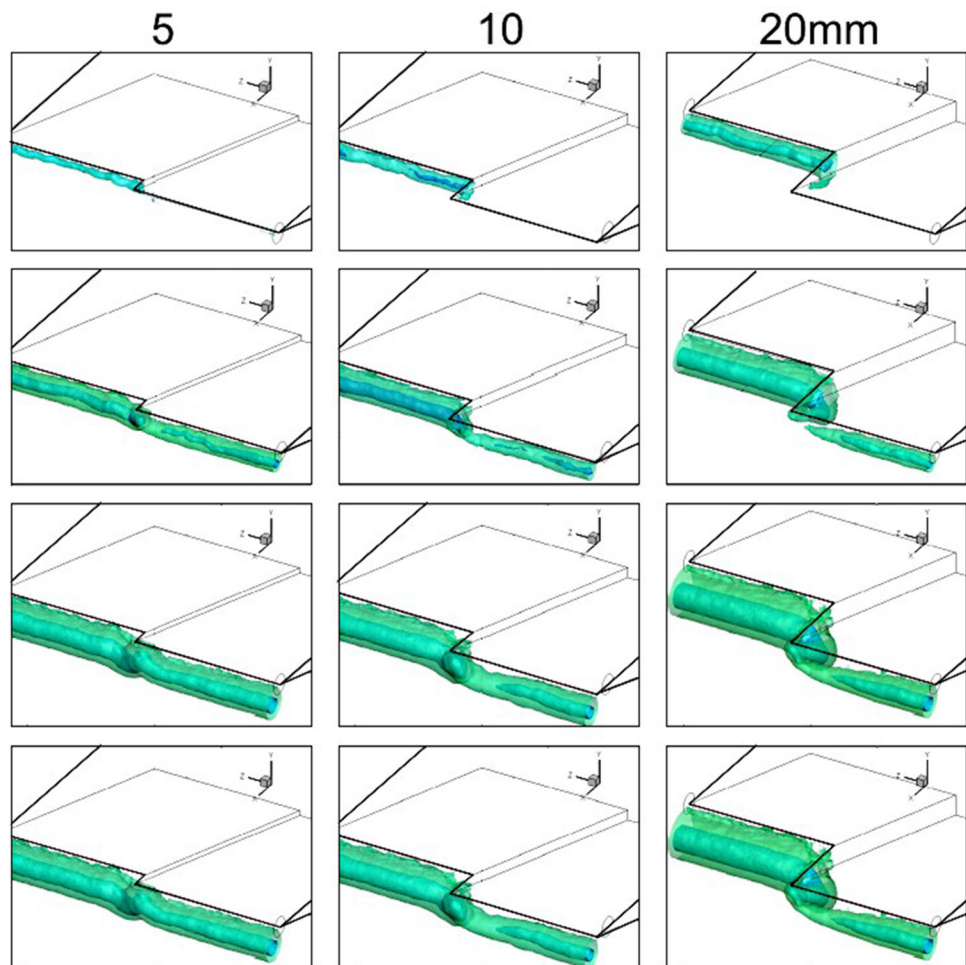

Fig. 12 Vorticity in the *x*–*y* plane situated at the offset edge for three offset edge lengths and times of 34 and 106 µs, and a Mach number of 1.42
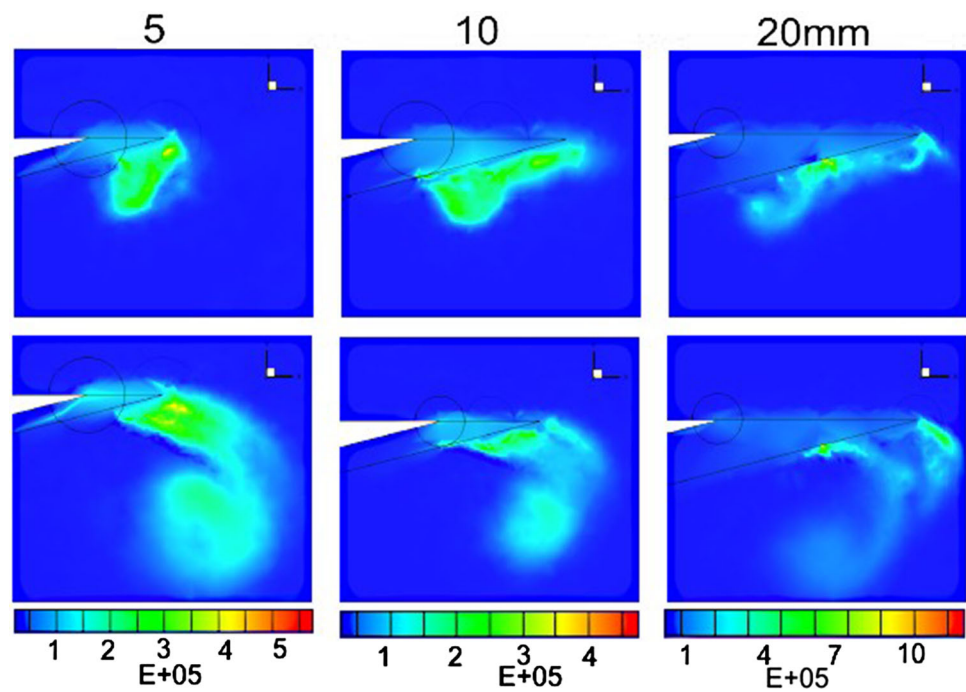
Fig. 13 Experimental
shadowgraph images of shock
diffraction for a Mach 1.6
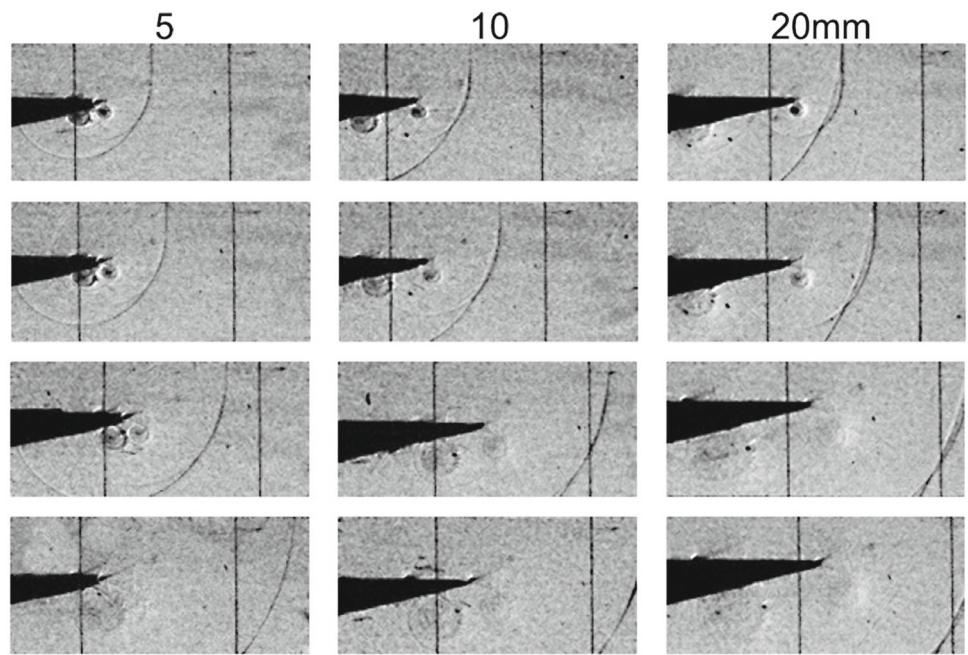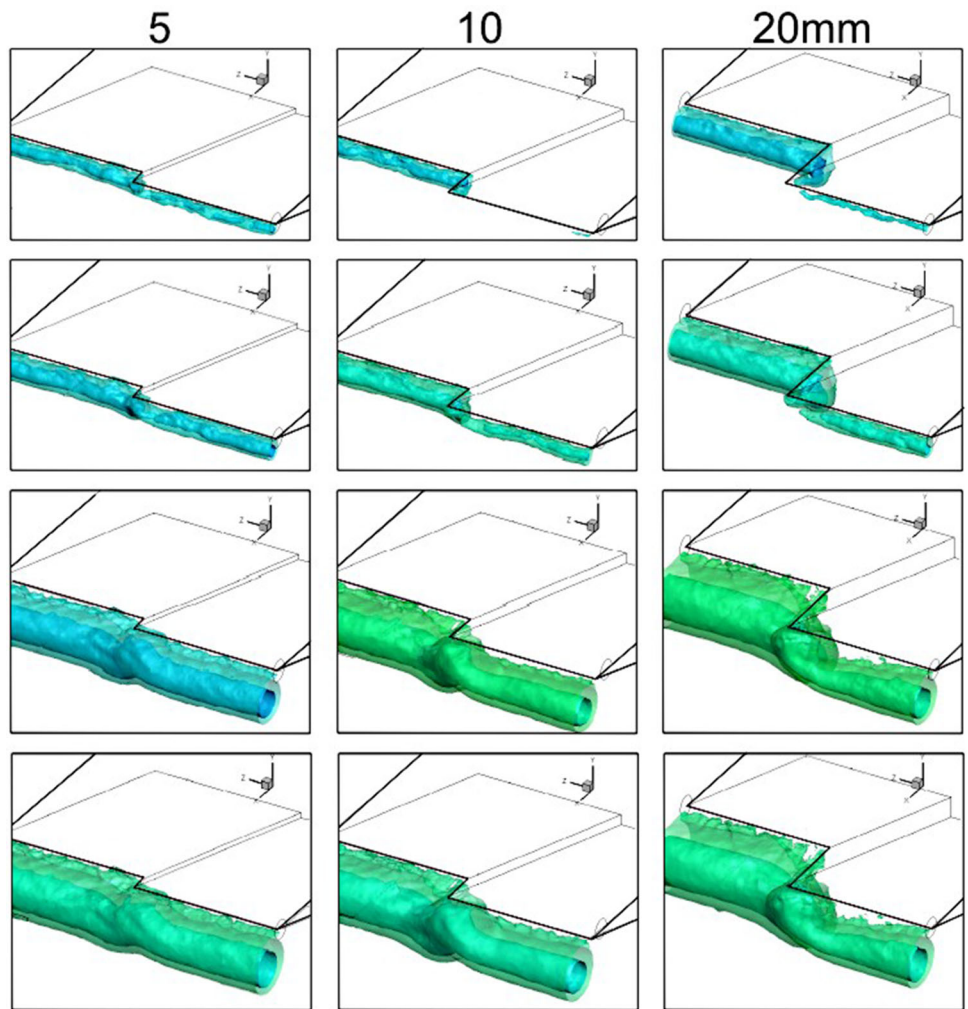incident shock wave at times of
16, 23, 39, and 55 μs

Fig. 14 Isosurfaces of density
of 0.8 kg/m^3 on the inner surface
and 1.1 kg/m^3 on the outer
surface, at time delays (*top* to
bottom rows) of 13, 29, 74, and
88 μs, at a Mach number of 1.60

show a decrease in diameter of the vortex tube from the downstream edge as it approaches the offset edge, as in the other cases, indicating a change in vorticity being influenced by the interaction between the two shed vortices. The vorticity plots are not presented for this case, since they are very similar to those for Mach 1.42, Fig. 12, although at earlier times because of the increased velocity.

4 Conclusion

A general and preliminary three-dimensional study of the merging of vortices resulting from shock diffraction over three edges is given. However a much more detailed high-resolution study is needed to clearly establish how the separate vortex cores wind around to the underside of the wedge and how they eventually combine.

References

1. Sun, M., Takayama, K.: Vorticity production in shock diffraction. J. Fluid Mech. **478**, 237–256 (2003)
2. Skews, B.W.: The perturbed region behind a diffracting shock wave. J. Fluid Mech. **29**, 705–719 (1967)
3. Sun, M., Takayama, K.: The formation of a secondary shock wave behind a shock wave diffracting at a convex corner. Shock Waves **7**, 287–295 (1996)
4. Reeves, J.O., Skews, B.W.: Unsteady three-dimensional compressible vortex flows generated during shock wave diffraction. Shock Waves **22**, 161–172 (2012)
5. Cooppan, S., Skews, B.W.: The interaction of three-dimensional compressible vortices. In: Proceedings of the 30th International Congress on High-Speed Imaging and Photonics, Pretoria, pp. 293–298 (2013)
6. Skews, B.W., Bentley, J.J.: Flows from two perpendicular shock tubes with a common exit edge. In: 21st International Shock Interaction Symposium, pp. 21–25. Riga, Latvia (2014)